

RESEARCH ARTICLE

Analysis of extracellular vesicle microRNA profiles reveals distinct blood and lymphatic endothelial cell origins

Marianne Pultar^{1,2,3} | Johannes Oesterreicher^{1,2} | Jaana Hartmann⁸ | Moritz Weigl^{1,2,3} |
Andreas Diendorfer³ | Katharina Schimek^{4,5} | Barbara Schädler^{1,2,9} | Thomas Heuser⁶ |
Marlene Brandstetter⁶ | Johannes Grillari^{1,2,7} | Peter Sykacek¹⁰ | Matthias Hackl³ |
Wolfgang Holnthoner^{1,2} 

¹Ludwig Boltzmann Institute for Traumatology, The Research Centre in Cooperation with AUVA, Vienna, Austria

²Austrian Cluster for Tissue Regeneration, Vienna, Austria

³TAmiRNA GmbH, Vienna, Austria

⁴Technische Universität Berlin, Medical Biotechnology, Berlin, Germany

⁵TissUse GmbH, Berlin, Germany

⁶Vienna Biocenter Core Facilities GmbH, EM Facility, Vienna, Austria

⁷Department of Biotechnology, Institute of Molecular Biotechnology, University of Natural Resources and Life Sciences, Vienna, Austria

⁸Hypericum Life Sciences GmbH, Vienna, Austria

⁹University Clinic of Dentistry, Medical University of Vienna, Vienna, Austria

¹⁰Department of Biotechnology, Institute of Computational Biology, University of Natural Resources and Life Sciences, Vienna, Austria

Correspondence

Wolfgang Holnthoner, Ludwig Boltzmann Institute for Traumatology, The Research Centre in Cooperation with AUVA, A-1200, Vienna, Austria.
Email: wolfgang.holnthoner@trauma.lbg.ac.at

Funding information

Austrian Ministry of Education, Science and Research

Abstract

Extracellular vesicles (EVs) are crucial mediators of cell-to-cell communication in physiological and pathological conditions. Specifically, EVs released from the vasculature into blood were found to be quantitatively and qualitatively different in diseases compared to healthy states. However, our understanding of EVs derived from the lymphatic system is still scarce. In this study, we compared the mRNA and microRNA (miRNA) expression in blood vascular (BEC) and lymphatic (LEC) endothelial cells. After characterization of the EVs by fluorescence-triggered flow cytometry, nanoparticle tracking analysis and cryo-transmission electron microscopy (cryo-TEM) we utilized small RNA-sequencing to characterize miRNA signatures in the EVs and identify cell-type specific miRNAs in BEC and LEC. We found miRNAs specifically enriched in BEC and LEC on the cellular as well as the extracellular vesicle level. Our data provide a solid basis for further functional in vitro and in vivo studies addressing the role of EVs in the blood and lymphatic vasculature.

KEYWORDS

extracellular vesicles, lymphatics, miRNA, vasculature

Marianne Pultar and Johannes Oesterreicher contributed equally to this study.

This is an open access article under the terms of the [Creative Commons Attribution-NonCommercial-NoDerivs License](https://creativecommons.org/licenses/by-nc-nd/4.0/), which permits use and distribution in any medium, provided the original work is properly cited, the use is non-commercial and no modifications or adaptations are made.

© 2024 The Authors. *Journal of Extracellular Biology* published by Wiley Periodicals, LLC on behalf of the International Society for Extracellular Vesicles.

1 | INTRODUCTION

Extracellular vesicles (EVs) are bilipid membrane enclosed nanoparticles and consist of three main subtypes differentiated by their biogenesis. Apoptotic bodies, microvesicles and exosomes are secreted by virtually all cell types and contain cell source specific cargo, such as proteins, lipids, metabolites and nucleic acids. Specific differences in their physical properties, including size, membrane composition and density allow for the enrichment of more refined subtypes of EVs (Théry et al., 2018). The cargo of vesicles was found to play a role in cell-to-cell communication in a paracrine manner (Milasan et al., 2016). Vesicles are transported mainly via the circulatory system and the respective body fluids such as blood and lymph fluid (Chen et al., 2012). In contrast to our knowledge on blood vascular-derived EVs, little is known about EVs derived from lymphatic endothelial cells (LEC) (Trisko et al., 2022).

During development the human vasculature forms two different vascular beds resulting in the blood and the lymphatic vessel system. The specific function of these two types of vasculature are reflected in their distinct anatomical structures, supported by endothelial cells (ECs) with differing phenotypic and molecular traits (Nelson et al., 2007). Whereas the blood vasculature's main role is the active distribution of blood and its components, the lymphatic system is responsible for the continuous removal of accumulating interstitial fluid (Oliver et al., 2020; Pugsley & Tabrizchi, 2000). Additionally, it fulfills a crucial role in the transport and interaction with immune cells (Randolph et al., 2017). Despite being clearly separated, both vessel types are embedded in close proximity to each other in different tissues, culminating in highly intertwined regions termed microvasculature. Especially in these regions the fluid and in consequence the molecular content exchange is a highly active process (Güven et al., 2020). With both the supply of blood and the removal of interstitial fluid being key for the development, and sustainment of higher organisms, and the imperative tissue homeostasis, diseases or damage of these systems result in tremendously detrimental effects (Cueni & Detmar, 2008; Flavahan, 2017). Since the first reported separation of blood and lymphatic ECs (BEC and LEC, respectively), our knowledge regarding their distinct roles and gene expression has been steadily extended (Kriehuber et al., 2001). Especially in the context of EC heterogeneity, studies have provided crucial evidence to decipher molecular processes driving disease progression (Greenspan & Weinstein, 2021; Gurevich et al., 2021; Lee et al., 2010). The analysis of endothelial cell mRNA profiles has led to important findings regarding endothelial identity in different tissues in homeostasis and pathological processes such as inflammation and cancer (Feng et al., 2019; Jambusaria et al., 2020; Pan et al., 2021). As an important part of the non-coding transcriptome, microRNAs (miRNAs), have been studied extensively in the field of vascular biology. Indeed, miRNAs stabilize the phenotype of LEC and BEC and are involved in the onset of the differentiation process (Dunworth et al., 2014; Jung et al., 2019; Pedrioli et al., 2010). Generally, these small non-coding RNA species, which typically consist of 20–30 nucleotides, can influence gene regulatory processes by different mechanisms such as targeting the 3' untranslated region (UTR) of mRNAs, leading to their degradation (Hammond et al., 2000; Treiber et al., 2019). Due to this regulatory effect, dysregulation of miRNA levels can lead to cellular dysfunction which allows for their potential use as diseases biomarker as well as therapeutic targets. The secretion of miRNAs is currently understood to follow three different mechanisms, passive leakage, active secretion as cargo in EVs, or by the formation and release of a miRNA-protein complex (Shah & Calin, 2013; Turchinovich et al., 2012).

In this study, the intracellular levels of miRNAs in blood and lymphatic ECs as well as the abundance of miRNAs in EV-enriched conditioned medium were investigated. We aimed to gain information on miRNA signatures specific for LECs and BECs as well as to identify miRNAs which are selectively secreted via EVs. Furthermore, we used mRNA sequencing to ensure lineage specificity of the used cell populations to prevent wrong classification and assignments of respective miRNAs. This study incorporates data that were generated and analysed in the course of a master's thesis (Pultar, 2022). Our results give first insights of the endothelial-specific miRNA patterns in EVs secreted by LEC and BEC. The correlation into the intracellular and extravesicular miRNA sequencing data on an absolute scale resulted in the identification of a subset of highly abundant miRNAs in EC-EVs. In conclusion, the here presented data holds great promise for future applications of EC-EV-derived miRNAs as biomarkers of various pathological processes as well as their role in determining EC heterogeneity.

2 | MATERIALS AND METHODS

2.1 | Cell culture

Human dermal microvascular endothelial cells (HDMEC) were isolated from the human foreskin, according to a protocol described previously (Schimek et al., 2013). Juvenile prepuce was obtained in compliance with the relevant laws, with informed consent and ethics approval (Ethic Committee Charité University Medicine, Berlin, Germany), from a paediatric surgery after routine circumcisions or were purchased from Promocell (Heidelberg, Germany). Human umbilical vein endothelial cells (HUVEC) were isolated from umbilical cords (Ethics Committee approval by the State of Upper Austria (#200)) according to standard procedures. Telomerase-immortalized lymphatic endothelial cells (LEC-Tert) were a kind gift from Dr. Marion Gröger (Medical University of Vienna, Austria). All cells were cultured in endothelial growth medium-2 (EGM-2, Lonza, Walkersville,

MD, USA) supplemented with 5% fetal calf serum (FCS, Sigma-Aldrich Co. LLC., St. Luis, MO, USA). The serum-supplemented growth medium is titled as full EGM-2 in further references.

Adipose stromal cells (ASC) were isolated from liposuction material as previously described (Priglinger et al., 2017; Wolbank et al., 2007) and cultured in full EGM-2 and used from single donors at passage 6 for EV-conditioning. Human dermal fibroblasts (HFF) purchased from Biomedica (Biomedica GmbH Vienna, AUT) HFF were cultivated in full EGM-2 and used at passages 3 and 7 for EV-conditioning.

2.2 | Fluorescent activated cell sorting (FACS)

3×10^5 HDMEC/cm² (passage 3) were seeded onto a T75 flask and cultured overnight. The next day the cells were detached using Accutase (Sigma) and transferred into a 15 mL falcon tube using FACS buffer (1 × phosphate-buffered saline (PBS) (w/o Ca⁺⁺ Mg⁺⁺) with 1% bovine serum albumin (BSA, Sigma-Aldrich Co. LLC., St. Luis, USA)). Cells were pelleted and washed with PBS at 500 × g for 5 min. Afterwards they were stained for 30 min on ice in the dark with anti-Podoplanin antibody (Monoclonal IgG1 Mouse Anti-Human D2-40 MCA2543, Bio-Rad Laboratories) 1:200 diluted in FACS buffer. Prior to the second staining with 1:500 diluted Alexa-Fluo-488 anti-mouse 2nd step antibody (Polyclonal IgG Goat Anti-Mouse Alexa Fluor™ 488, Thermo Fisher Scientific Inc) in FACS buffer, cells were washed with PBS (w/o Ca⁺⁺ Mg⁺⁺). Staining was performed for 30 min on ice in the dark. 2 μL CD31-PE (Mouse Anti-Human PE, MBC 78.2, BD Biosciences) in FACS buffer were added to the cell pellet and incubated for another 30 min on ice. Double-stained cells were washed with PBS and re-suspended in 300 μL FACS-Buffer. The resuspended cells were stored on ice and applied on a cell strainer prior to the sorting on a BC MoFlow Astrios EQ (Beckman Coulter, Brea, California, USA). The gates were set to sort PE-positive events only to make sure to not co-sort CD31-negative fibroblasts or other non-endothelial cells. The PE-positive events were further sub-gated into Alexa-Fluo-488 positive cells, expressing Podoplanin. Cells were directly sorted in 5 mL full EGM-2 and seeded onto a T25 flask.

2.3 | EV-conditioning of cells

3×10^5 cells/cm² of EC (passage 7) were seeded onto 2 × T75 and 3 × T25 flasks using full EGM-2. The medium was changed every 2–3 days until cells reached confluency. Cells were kept confluent 48 h before they were washed trice with PBS (w/o Ca⁺⁺ Mg⁺⁺) and 12 or 4 mL endothelial basal medium (EBM-2, Lonza, Walkersville, MD, USA) were added for conditioning of T75 or T25 flasks, respectively. One T25 flask was used to count and characterise cells prior to the conditioning. After 24 h conditioned medium from 2 × T75 and 2 × T25 was collected and pooled. Conditioned cells were detached using Accutase and PBS (w/o Ca⁺⁺ Mg⁺⁺), pooled and split up into aliquots for the preparation of whole cell lysates, isolation of RNA, estimation of cell number and surface marker profile of the cells. For the isolation of RNA, cell numbers equivalent to 75 cm² of cell layer were used. For the inclusion of non-endothelial control groups HFF and ASC were cultured in T75 flasks using EGM-2 until 70%–80% confluence. Washing and conditioning were performed as described for the endothelial cells.

2.4 | Characterization of cells

Different endothelial cell types were characterized by standard flow cytometry and immunoaffinity staining using a Cytotflex flow cytometer (Beckman Coulter GmbH, Brea, CA, USA). After conditioning cells were detached from cell culture flasks by washing two times with 1 × PBS (w/o Ca⁺⁺ Mg⁺⁺) and incubation for 5 min at 37°C and 5% CO² with added 1 × Accutase (Sigma-Aldrich Co. LLC., St. Luis, USA). Cells were collected with full EGM-2 (EGM-2, Lonza, Walkersville, MD, USA). Samples were centrifuged at 300 × g for 5 min and washed with 1 × PBS (w/o Ca⁺⁺ Mg⁺⁺). Cells were resuspended in FACS buffer and splitted into separate aliquots for individual stainings. Immunoaffinity staining with antibodies was done for Podoplanin (Monoclonal IgG1 Mouse Anti-Human D2-40 MCA2543, Bio-Rad Laboratories, Hercules, CA, USA) in combination with a second step antibody (Polyclonal IgG Goat Anti-Mouse Alexa Fluor™ 488, Thermo Fisher Scientific Inc., Waltham, MA, USA), CD31/PECAM (Mouse Anti-Human PE, MBC 78.2, BD Biosciences, Franklin Lakes, NJ, USA), VE-Cadherin (VECAD) (Anti-Human FITC, BD Biosciences, Franklin Lakes, NJ, USA) and vascular endothelial growth factor receptor 2 (VEGFR2) (Anti-Human PE, BD Bioscience, Franklin Lakes, NJ, USA). Antibodies were diluted in FACS buffer before addition to the cells and incubation in the dark for 30 min at 4°C. After incubation with respective antibodies, samples were washed by addition of 1 mL 1 × PBS (w/o Ca⁺⁺ Mg⁺⁺) and centrifugation at 300 × g for 5 min before resuspension in FACS buffer. Appropriate controls for performed measurements included unstained, single stained, second step only as well a PE isotype control (IgG Mouse Isotype Control PE, BD Biosciences, Franklin Lakes, NJ, USA and IgG Mouse Isotype Control FITC, BD Biosciences, Franklin Lakes, NJ, USA). Before sample analysis, the flow cytometer was performance-checked by the quality control protocol stated by the manufacturer.

2.5 | Enrichment for EVs

Around 32 mL of pooled conditioned medium were centrifuged at $500 \times g$ for 5 min at RT, followed by a centrifugation step at $2000 \times g$ for 5 min at RT. The supernatant (S2) was transferred in fresh tubes and further centrifuged at $10,000 \times g$ for 30 min at 4°C in a Heraeus Megafuge 16R (Thermo Fisher Scientific, Waltham, MA, USA). The resulting supernatant (S10) was used to concentrate small EVs by a centrifugation step at $100,000 \times g$ for 65 min at 4°C using a Optima™ C-100 XP ultracentrifuge (Beckman Coulter GmbH, Brea, CA, USA). The EV pellet after the $10,000 \times g$ centrifugation step (P10) was resuspended in $240 \mu\text{L}$ $0.22 \mu\text{m}$ -filtered PBS (w/o Ca^{++} Mg^{++}) whereas the EV pellet containing the small EVs (P100) was resuspended in $400 \mu\text{L}$ PBS (w/o Ca^{++} Mg^{++}). The supernatant from the final $100,000 \times g$ centrifugation (S100) was used as a control of the enrichment process. The P100 fraction was split into aliquots for RNA isolation (volume corresponds to 90 cm^2 of confluent mono cell layer), characterisation (volume corresponds to 45 cm^2 of confluent mono cell layer) and cryogenic electron microscopy (volume corresponds to 65 cm^2 of confluent mono cell layer).

2.6 | Handling and storage of EVs

All experimental steps and storage of EV samples were performed using DNA-LoBind microtubes (Eppendorf, Hamburg, Germany). To avoid bias due to the handling of EV samples, enrichment procedure, storage time and freeze thaw cycles were done in the same manor for all samples. Characterisation via nanoparticle tracking analysis (NTA) and fluorescence-triggered flow cytometry (FT-FC) was performed on fresh samples (no freeze thaw cycle). NTA was done 24–26 h, FT-FC was done 48–50 h after ultracentrifugation (UC) enrichment and storage at 4°C . RNA isolation as well as cryo-TEM were conducted after one freeze thaw cycle (storage -80°C in low binding tubes).

2.7 | Nanoparticle tracking analysis (NTA)

Size distribution and concentration of particles were assessed by NTA using a ZetaView PMX110 device from Particle Metrix (Zeta VIEW S/N 239, software ZetaView 8.04.02, camera $0.703 \mu\text{m}/\text{px}$, Cell S/N: CA0058-0109, Particle Metrix, Meerbusch, Germany) by differential ultracentrifugation EV-enriched cell culture supernatant samples as described before (Oesterreicher et al., 2020). In brief, samples were diluted into a total volume of $1500 \mu\text{L}$ pre-filtered ($0.22 \mu\text{m}$ PVDF syringe filter) $1 \times$ PBS (w/o Ca^{++} Mg^{++}) to obtain detection rates recommended by the manufacturer when applicable. Camera and acquisition settings were chosen as following, shutter 50, sensitivity 80, minimal brightness 20, minimal area 10 and maximal area 1000 with 11 positions.

2.8 | Fluorescence-triggered flow cytometry (FT-FC) for EV characterisation

EV-enriched samples were analysed for their lipid membrane and antigen representation by FT-FC as described previously (Oesterreicher et al., 2020). In brief, $10 \mu\text{L}$ of via differential ultracentrifugation obtained samples were added to $70 \mu\text{L}$ filtered ($0.22 \mu\text{m}$ PVDF syringe filter) $1 \times$ PBS (w/o Ca^{++} Mg^{++}) and stained for presence of a lipid membrane by addition of $20 \mu\text{L}$ Cell Mask Green (CMG) (Thermo Fisher Scientific, Waltham, MA, USA) which was pre-diluted 1:2000 in filtered ($0.22 \mu\text{m}$ PVDF syringe filter) $1 \times$ PBS (w/o Ca^{++} Mg^{++}). Samples were then incubated for 30 min at 37°C in the dark. Staining of respective antigens was performed by addition $1 \mu\text{L}$ directly PE-conjugated antibodies for CD63, CD81 (Clones REA1055 and REA513, Miltenyi Biotec, Bergisch Gladbach, Germany) and CD31 (Clone WM59, BD Pharmingen). Incubation was done for 30 min at room temperature in the dark. Samples were measured using a calibrated Cytoflex flow cytometer (Beckman Coulter GmbH, Brea, CA, USA) with the event trigger set to 3000 for the FITC channel and a flow rate of $10 \mu\text{L}/\text{min}$. Controls performed included unstained, single stained and IgG PE isotype controls as well as lysed samples.

2.9 | Cryo-electron microscopy

Quantifoil (Quantifoil Micro Tools GmbH, Großlöbichau, Germany) holey carbon copper grids (Cu 200 mesh, R 1.2/1.3; hole diameter: $1.2 \mu\text{m}$, hole spacing: $1.3 \mu\text{m}$) were glow discharged for 240 s, mounted on forceps, and loaded into the climate chamber of a Leica EM GP grid plunger (Leica Microsystems, Wetzlar, Germany) set to 4°C and 85% humidity. After application of $4 \mu\text{L}$ of EV fraction ($400 \mu\text{g}/\text{mL}$ final concentration) grids were blotted with filter paper (Whatman filter paper #1, Little Chalfont, Great Britain) 1 to 4 s from the front side and rapidly frozen in ethane at approximately -180°C for instant vitrification. Samples

were kept at liquid nitrogen until examined with a 200 kV Glacios cryo-transmission electron microscope (Thermo Scientific, Waltham, MA, USA) equipped with an extra bright field emission gun and a Falcon3 direct electron detector operated in linear mode. Digital images were recorded at a magnification of 150,000-fold with a pixel size of 0.99 Å, a defocus of $-2 \mu\text{m}$ and a total electron dose of $60 \text{ e}/\text{Å}^2$ (Dittrich et al., 2022).

2.10 | Isolation of cellular and vesicular RNA

Total RNA from cells and EVs was isolated using the miRNeasy Kit from Qiagen (Qiagen, Hilden, Germany) following the manufacturer's instructions. To isolate RNA, cells equivalent to 37.5 cm^2 were lysed in Qiazol and automatically isolated via a Qiacube (Qiagen, Hilden, Germany) based protocol. $90 \mu\text{L}$ of the pooled P100 fraction of enriched EVs, which is equivalent to the EVs derived from 90 cm^2 of cells, were filled up to $200 \mu\text{L}$ using $0.22 \mu\text{m}$ filtered PBS and stored at -80°C until RNA isolation. Prior to the automatic RNA isolation using the Qiacube, EVs were lysed with Qiazol containing synthetic RNA spike ins and glycogen was added to the aqueous phase at a final concentration of $50 \mu\text{g}/\text{mL}$. Concentration and quality of the eluted RNA were investigated using the Nanodrop (Thermo Scientific, Waltham, MA, USA) and Bioanalyzer Agilent RNA 6000 Nano Kit (Agilent, Santa Clara, CA, USA) for the cellular RNA. Due to the low RNA content in EV samples, the RNA concentration and profiles were estimated using the Bioanalyzer Agilent RNA 6000 Pico Kit (Agilent, Santa Clara, CA, USA).

2.11 | Quantitative PCR (qPCR) validation

Reverse transcription (RT) was performed using the miRCURY RT kit (Qiagen, Venlo, Netherlands). For cDNA synthesis $2 \mu\text{L}$ total RNA from EVs or 100 ng total RNA from cells with additional $1 \mu\text{L}$ cDNA spike in (cel-miR-39-3p) per reaction were used. qPCR was performed using the miRCURY SYBR[®] Green Master Mix with commercial LNA-enhanced miRNA assays (Qiagen) and a final cDNA dilution of 1:100 for cell samples and 1:20 for EV samples. qPCRs were performed on a LightCycler480 II (Roche) with the following settings: 95°C for 2 min, 45 cycles of 95°C for 10 s and 56°C for 60 s. Melting curve analysis was performed using continuous acquisition between 55°C and 99°C . Cycle threshold (Cq) values were calculated with the 2nd derivative maximum method (LC480, Roche v1.5.1.62). cDNA (cel-miR-39-3p) and PCR (UniSp3) spike-ins were measured in all samples (Figure S4b). For EV samples RNA (UniSp4) was measured in addition. Cq values were normalized with miR-140-3p, as it was found to be highly correlated on EV and cell levels within matching samples (Figure 5c,d).

2.12 | In situ hybridization of miRNAs

Written informed patient consent was obtained before tissue collection in accordance with the Declaration of Helsinki, and with approval from the Institutional Review Board of the Medical University of Vienna under the ethical permits EK#1695/2021 and EK#1783/2020 granted to our collaborator BML. For localization of the different miRNA within human skin, we did four consecutive tissue sections in $4 \mu\text{m}$ thickness. The sections were stained for either CD31 (1:2000, Abcam, ab182981, Cambridge, UK) or Podoplanin (1:40, BioRad, MCA 2543, Hercules, USA) for immunofluorescent histochemistry. For miRNA detection, the sections were processed following the protocol for miRNAscope[™] Assay red (ACD Bio, 324500, Newark, USA). The sections were fixed and pretreated to perform target retrieval in several steps. For incubation with the two different probes for miR-150-5p-S1 (ACD Bio, 108755-S1, Newark, USA) or miR-378a-3p-S1 (ACD Bio, 729191-S1, Newark, USA) the sections were placed in the hybridization oven for 2 h at 40°C . Afterwards, several amplification steps were performed. The nuclei staining of the tissue was performed with DAPI.

2.13 | Small RNA sequencing

RealSeq[®]-Biofluids library preparation kit (RealSeq Biosciences, Santa Cruz, CA, USA) was used to prepare a small RNA library of cellular and vesicular RNA. A fixed amount of 200 ng total RNA from cells and a fixed volume of $8.5 \mu\text{L}$ total RNA from EVs was used as input. To later allow for absolute normalization of small RNA sequencing data $1 \mu\text{L}$ of miND[®] spike-in (TAmiRNA, Vienna, Austria) (Khamina et al., 2022) was added to the purified RNA. EV libraries were prepared using a 1:3 adapter dilution and 21 cycles in the PCR. For the cell libraries, the adapter was used undiluted, and 19 PCR cycles were performed. DNA libraries containing a barcode sequence were quantified using the Bioanalyzer Agilent DNA 1000 Kit (Agilent, Santa Clara, CA, USA), to prepare equimolar pools of EV and Cell samples (2×12 plex pool). Pools were purified using a microfluidic 3% agarose gel cassette (Sage Biosciences, Beverly, MA, USA), selecting for a size range between 130 and 160 bp to deplete adapter dimers and

enrich for 'microRNA-sized' inserts. Two lanes of an Illumina HiSeqV4 SR50 (Illumina, San Diego, CA, USA) were used for sequencing.

2.14 | mRNA sequencing

QuantSeq 3' mRNA-Seq Library Prep Kit FWD for Illumina (Lexogen GmbH, Vienna, Austria), was used to prepare mRNA libraries from 250 ng cellular RNA. DNA libraries were amplified by a 17 cycle PCR and their concentration was measured using the Bioanalyzer Agilent High Sensitivity DNA Kit (Agilent, Santa Clara, CA, USA). An equimolar 12-plex pool was prepared. Libraries were sequenced on an Illumina HiSeqV4 SR50 (Illumina, San Diego, CA, USA).

2.15 | Analysis of NGS data

Small RNA sequencing was analysed using the miND Pipeline (Diendorfer et al., 2022). FastQC v0.11.9 (Simon, 2010) and multiQC v1.10 (Ewels et al., 2016) were used to check the quality of the raw as well as the pre-processed data. Cutadapt v3.3 was used to trim the RealSeq adapter sequence for smallRNA sequencing derived reads and further filter reads with a quality score below 30 and shorter than 17 nt. For mRNA sequencing data the trimming and filtering was conducted using bbmap and the function bbduk v38.90 (Bushnell, 2014), whereas the same cut-offs as for sRNA pre-processing were set. Small RNA sequencing data was mapped against the human genomic reference GRCh38.p12 provided by Ensembl (Zerbino et al., 2018) using bowtie v1.3.0 (Bushnell, 2014). All mapping reads were further processed by miRDeep2 v2.0.1.2 (Friedländer et al., 2008) by being mapped against miRBase v22.1 (Griffiths-Jones et al., 2008) allowing for one mismatch and filtering for human-specific miRNAs (hsa). All genomic non-miRNA-related reads were investigated for the general RNA composition using bowtie v1.3.0 (Bushnell, 2014) and RNAcentral (The RNAcentral Consortium, 2019).

mRNA sequencing data was first mapped against the human genomic reference GRCh38.p12 provided by Ensembl (Zerbino et al., 2018) using STAR v2.7.7a (Dobin et al., 2013). Feature counts were generated using HTSeqCount v0.12.4 (Putri et al., 2022). For statistical analysis, as well as data visualization R v4.0 and Bioconductor packages were used. Differential expression was performed using edgeR v3.32 (Robinson et al., 2010) and the independent filtering method of DESeq2 (Love et al., 2014) was adapted in order to remove low abundant miRNAs/mRNAs and work with edgeR.

2.16 | Gene set enrichment analysis

Gene ontology (GO) term enrichment analysis was performed using the R package topGO v2.50.0 (Adrian Alexa, 2017). GO Annotation for biological processes was derived for human from org.Hs.eg.db v3.16.0 (Carlson, 2017). Kolmogorov Smirnov (KS) test statistic was used for data derived from the mRNA sequencing experiment. Gene subsets were created for upregulated mRNAs in either BEC or LEC. The unadjusted *p*-value from the edgeR differential expression analysis was used as a weight in the KS statistic.

A similar statistical approach was used for the intracellular miRNA sequencing experiment, expect that gene subsets were derived differently. To get possible interacted target mRNAs, the overlap of downregulated mRNAs with the targets of upregulated miRNAs within one cell type was used. The respective *p*-values for those genes were derived from the mRNA differential expression analysis.

GO enrichment analysis for differentially expressed extravesicular miRNAs as well as the top EV-enriched miRNA subset is based on predicted target genes only. To test for enrichment, all annotated genes were used as a reference whereas only predicted targets were marked as detected for the Fisher hypergeometric test.

Based on the unadjusted *p*-value derived from the GO enrichment, the top significantly identified biological processes are visualized with ggplot2 v3.4.2 as a dot plot.

2.17 | Target prediction

Target prediction was performed using the R package miRNAtap v1.32.0 (Maciej Pajak, 2017). Predicted targets were derived from five different sources (DIANA (Maragkakis et al., 2009), TargetsScan (Agarwal et al., 2015), PicTar (Lall et al., 2006), Miranda (Griffiths-Jones et al., 2008) and miRDB (Wong & Wang, 2015)). The aggregated rank product was calculated based on the geometric mean for all targets which were found in at least two individual databases.

Interactions between mRNAs and miRNAs are visualized in a circos plot using the R package circlize v0.4.15 (Gu et al., 2014).

3 | RESULTS

3.1 | Phenotype and genotype of blood vascular and lymphatic endothelial cells

To acquire primary lymphatic and blood endothelial cells to study the intra- and extracellular transcriptome, HDMEC were used to obtain monocultures of LEC and BEC. Fluorescence activated cell sorting (FACS) resulted in a CD31+/Podoplanin- (PDPN) (BEC) and CD31+/ PDPN + (LEC) cell population. In total five pure LEC and two pure BEC as well as two different mixtures of BEC and LEC were used for this study. HUVEC and telomerase-immortalized LEC were used as additional controls. All donors/cells are marked in different colours and labelled 'A'–'K'. To avoid media component-derived EV contamination, plain endothelial basal medium (EBM-2) was used to harvest EVs. Therefore, cells were characterized before and after conditioning to monitor biases due to potential changes of their phenotype. Despite the potential stress of starvation and supplement restriction during the conditioning process, the surface marker profile of the cells remained lineage specific. No changes in the expression of endothelial markers CD31 and VE-Cadherin (VECAD) were detected and podoplanin was observed exclusively on LEC (Figure S1). Except for telomerase-immortalized LEC, vascular endothelial growth factor receptor 2 (VEGFR2) was present on the cell surface of all other cell types, irrespective of the medium switch.

To characterize the transcriptome of the different EC types, that were used to derive EC specific EVs, the levels of intracellular mRNAs were investigated by 3' mRNA sequencing. Unsupervised hierarchical clustering over prefiltered mapped mRNAs indicates lineage specific expression patterns for LEC and BEC. The expression of mRNAs of the primary cell types (LEC, BEC and HDMEC) differs from the one of HUVEC and LEC-tert (Figure 1a). Differential gene expression analysis (false discovery rate (FDR) < 0.05) revealed 551 genes to be enriched in pure LEC ($n = 5$) and 394 enriched genes in pure BEC ($n = 2$, Figure 1b). Previously reported lymph-specific genes such as podoplanin (PDPN) and Prospero homeobox protein 1 (PROX1) were found to be higher expressed in LEC with a log fold change (logFC) of 6.2 and 4.7, respectively (Figure 1b). The expression levels of PDPN and PROX1 are low in BEC samples, with less than 0.1 and 13 RPM (Figure 1c). Vascular endothelial growth factor C (VEGFC), which is known to be highly expressed by endothelial cells of the blood vasculature, was lower expressed in LECs compared to BECs (logFC < -2.9) (Figure 1b). A GO-Term enrichment analysis based on upregulated genes in BEC revealed biological processes tightly associated with the vascular system (colour-highlighted, among others), under the top 30 GO-terms that were found to be significantly enriched (Figure 1d). The top 30 significantly enriched biological processes derived from a GO-term enrichment analysis based on upregulated mRNAs in LEC showed several coagulation and wound healing associated terms (Figure 1e).

3.2 | Intracellular miRNA expression discriminates LEC from BEC

To investigate the differences in miRNA transcription between LECs and BECs, small RNA sequencing was performed. Between 9.5 and 27 million (Mio) reads were obtained by small RNA sequencing of intracellular RNA. At least 92% mapped against the human genome and between 29% and 69% were identified to be miRNAs by mapping against the miRBase reference. Between 913 and 1282 different miRNAs were detected in each sample (Figure S3a,b). At a minimum, 460 different miRNAs with a read count above 10 were identified in every sample. Unsupervised hierarchical clustering of prefiltered miRNAs showed a close relation of three LEC donors. The second cluster was formed by two sub-clusters one containing the remaining two LEC donors and one consisting of the BEC donors (Figure 2a). Differential expression of identified miRNAs between LEC and BEC revealed 17 intracellular miRNAs to be upregulated and 13 to be downregulated in LEC with an FDR < 0.05 (Figure 2b). Among others, miRNAs 483-5p, 483-3p, 135-5p and 155-5p were enriched in BEC, whereas miRNAs 99a-5p, 511-5p, 146a-5p, 551a and 378a-3p were enriched in LEC (Figure 2b,c). Target prediction of the differentially expressed miRNAs showed several interactions between upregulated miRNAs in one EC type and their associated downregulated mRNAs. For both cell types, genes targeted by three different miRNAs were found. For BEC, mir-92b-3p was observed to interact with the largest number of downregulated mRNAs, whereas 26 out of 45 target genes were found to be uniquely targeted by this miRNA. In LEC, mir-148a-3p was identified as the miRNA with the most interactions. From 15 down regulated target mRNAs of these LEC enriched miRNA, 8 were found to be uniquely targeted by mir-148a-3p (Figure 2d). Based on the overlap of identified target mRNAs for the individual miRNAs and downregulated mRNAs, GO term enrichment analysis was performed for LEC and BEC. Under the top significantly enriched biological processes (BPs) for LEC specific downregulated interacted mRNAs, we found several vascular biology related terms (highlighted in orange, Figure 2e). For the BEC related analysis we did not find any vascular biology related BPs (Figure 2f).

3.3 | Characterization of BEC and LEC enriched EVs

Under physiological conditions ECs in vitro are growing in a confluent monolayer forming a cobblestone like pattern. Confluent cells were used to collect conditioned medium that is further used for differential ultracentrifugation to enrich for EVs.

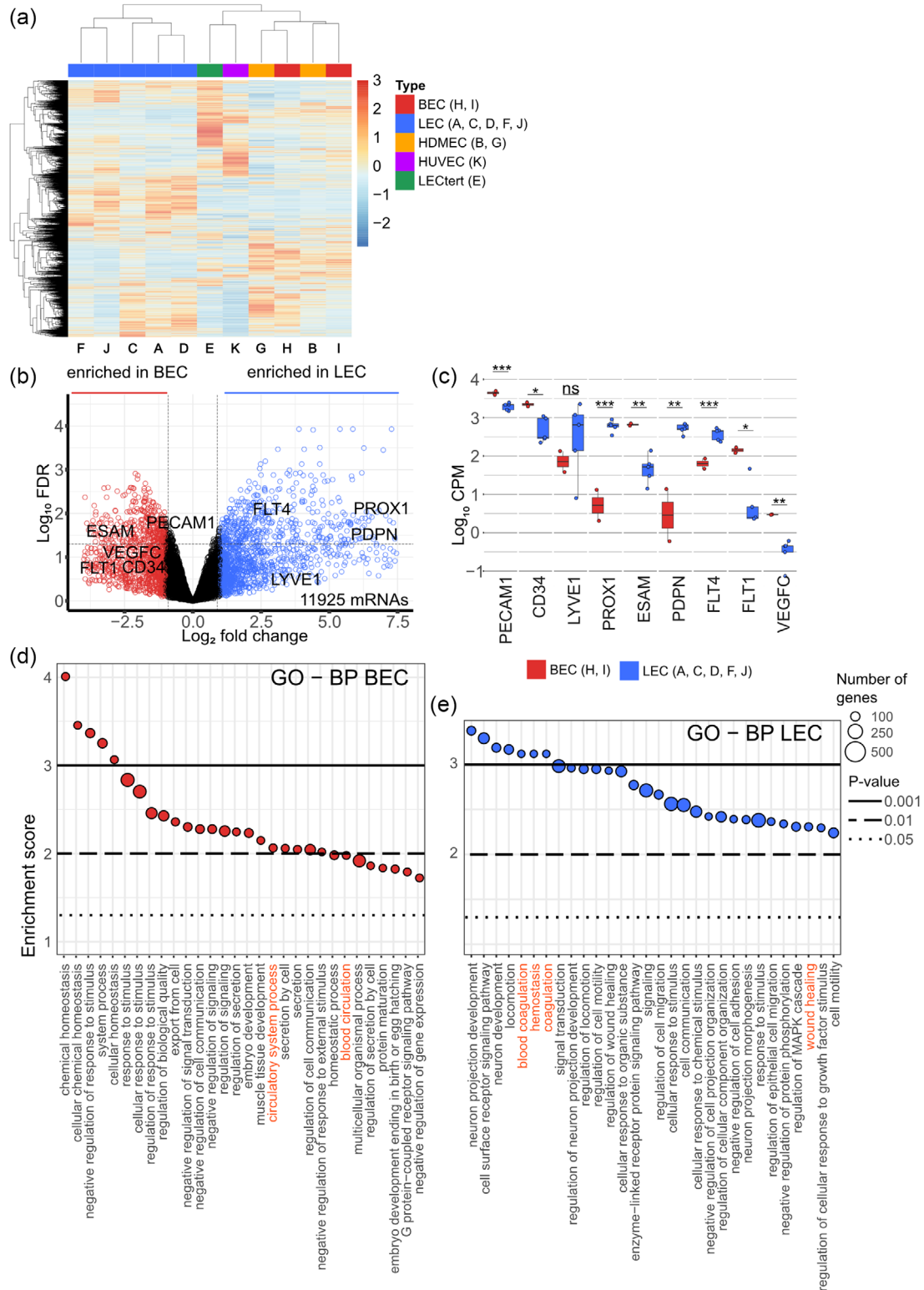


FIGURE 1 Intracellular mRNA expression. (a) Unsupervised hierarchical clustering of mRNA expression for LEC ($n = 5$), BEC ($n = 2$), HDMEC ($n = 2$), HUVEC ($n = 1$) and LEC-tert donor ($n = 1$). Clustering is based on filtered RPM values. Colour indicates the cell type. (b) Volcano plot of differential expression of mRNAs between LEC ($n = 5$) and BEC ($n = 2$) donors. \log_2 fold change (\log_2 FC) and \log_{10} false discovery rate (\log_{10} FDR) are plotted for 11,925 mRNAs. Coloured mRNAs were found with a \log_2 FC < -1 or > 1 between BEC and LEC (red and blue, respectively). Dashed lines are indicating a FDR > 0.05 and a \log_2 FC < -1 or > 1 . Selected target mRNAs are labelled. (c) Box plots of the expression of selected targets. Counts per million are visualized on a log scale for LEC and BEC (blue and red, respectively). Statistics are derived from edgeR (ns $p > 0.05$, * $p < 0.05$, ** $p < 0.01$, *** $p < 0.001$, **** $p < 0.0001$). GO-Term enrichment analysis of biological processes based on upregulated genes in (d) BEC and (e) LEC. Top 30 GO-terms found to be enriched for the differentially expressed mRNAs and their enrichment score (log p -value based on Kolmogorov Smirnov) and the number of annotated genes per GO-Term are plotted. Biological processes related to vascular biology are highlighted in orange.

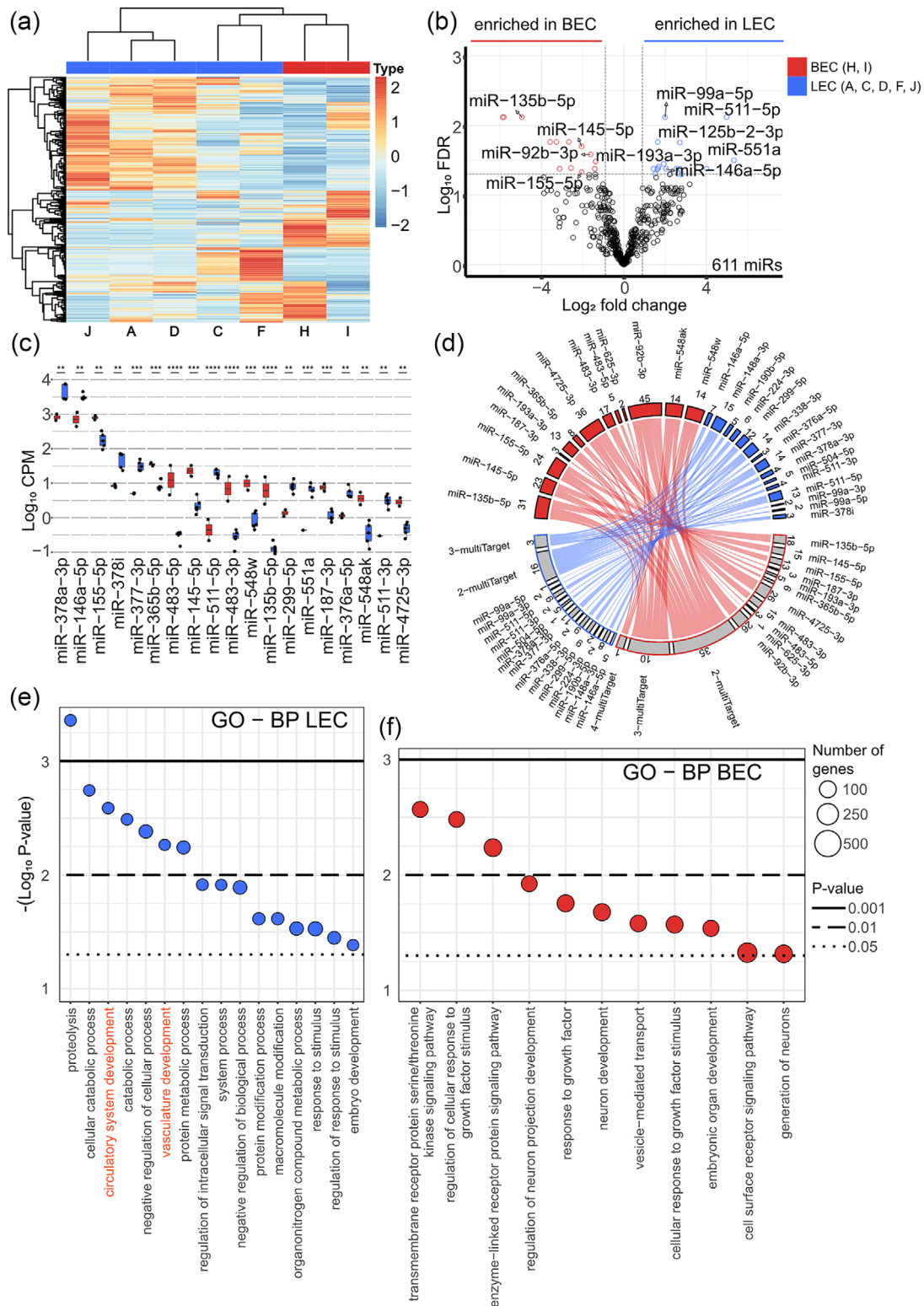


FIGURE 2 Intracellular miRNA expression. (a) Unsupervised hierarchical clustering of miRNA expression for LEC ($n = 5$) and BEC ($n = 2$) donors. Clustering is based on unit variance scaled RPM values. Cell type is colour coded on the horizontal clusters. (b) Volcano plot of differential expression of miRNAs between five LEC and two BEC donors. Log_2 fold change (logFC) and log_{10} false discovery rate (logFDR) are plotted for 611 miRNAs. Coloured miRNAs were found with a $\text{logFC} < 1$ or > 1 between BEC and LEC (red and blue, respectively) and a $\text{FDR} < 0.05$. Dashed lines indicate an FDR of 0.05 and a logFC of -1 or 1 . (c) Box plots of the expression of miRNA with an absolute logFC greater than 2. Counts per million are visualized on a log scale for LEC and BEC (blue and red, respectively). Statistics are derived from edgeR (ns $p > 0.05$, * $p < 0.05$, ** $p < 0.01$, *** $p < 0.001$, **** $p < 0.0001$). (d) Circos plot visualizing the interaction between upregulated miRNAs in BEC (red) and the corresponding downregulated target mRNAs in BEC (grey with red border). The same is shown for upregulated LEC miRNAs (blue) and downregulated target mRNAs in LEC (grey with blue border). Target mRNAs are summarized by the number

(Continues)

FIGURE 2 (Continued)

of interacting miRNAs (e.g., 3-multiTarget contains genes that are targeted by three different miRNAs) and the number of genes per group is provided next to the track. GO-term enrichment analysis of biological processes based on the downregulated interacted mRNAs in (e) LEC and (f) BEC. Top 30 GO-terms found to be enriched for the differentially expressed miRNAs and their regulated predicted targets their enrichment score (log *p*-value based on Kolmogorov Smirnov) is shown. Size of the circle indicated the number of annotated genes per GO-Term. Biological processes related to vascular biology are highlighted in orange.

Three sample types were collected: (i) the supernatant of the ultracentrifugation (S100), (ii) the pellet containing larger EVs (P10) and (iii) the pellet containing small EVs (P100). All samples were then characterized by determining their size, concentration and marker profile using nanoparticle tracking (NTA) and FITC-triggered flow cytometry (FT-FC). NTA showed successful enrichment of small extracellular particles (EPs) for all cell types, as the concentration of nanoparticles per mL was higher in the P100 fraction compared to S100 and P10 (Figure S2a). NTA identified significantly fewer EPs in P10 and P100 from LEC samples compared to BEC (Figure 3a). The mean size of the small EV fraction (P100) showed a narrower size range of particles with a peak at around 100 nm compared to the more heterogeneous population of EPs in the P10 fraction. The mean size of P100 was significantly smaller compared to the one of P10 for all cell types (Figure 3b,c). No significant difference was observed in the average particle size between LECs and BECs. FT-FC analysis confirmed the higher abundance of lipid-enclosed particles in P100 compared to P10 (Figure 3d). The mean of CMG positive EVs in the S100 supernatant, over all CMG-stained measured samples, was 70- and 80-fold lower compared to the concentration detected in P100 and P10, respectively. A significantly 3- (P10) or 2-fold (P100) higher concentration of EV/mL in BEC samples was detected compared to LEC (Figure 3d). Surface marker presence on EVs was checked using a double staining approach of CMG and fluorescence-labelled antibodies. The geometric mean fluorescent intensity was investigated and revealed that CD63 and CD81 are present on both EVs enriched in P10 and P100 fractions for both cell types. CD31 was only detected in low amounts on large BEC-enriched EVs (P10) (Figure 3e).

The EV size was estimated in accordance with three different size range gates, ranging from small EVs (smaller than 200 nm), intermediate EVs (200–500 nm) to large EVs (bigger than 500 nm). The approximation of the size of EVs reveals that the highest percentage from all detected events in the EV total gate was in the small EV gate for all different fractions. The percentage of EVs smaller than 200 nm was significantly higher in P100 and P10 fraction of LEC compared to BEC with approximately 80% of all EVs being small ones (Figure 3f). Density scatterplots of measured stained EVs and their fluorescent intensity in the FITC-channel versus the signal detected in the SSC-channel visualized an EV population with the highest event count in the small EV gate (light grey) (Figure 3g). Most of the detected events were in the EV total gate (black) except for some CMG-positive events which showed a different scattering property. As a result, the gating was applied under the assumption that the fluorescent intensity is increasing with respect to the size of spherical EVs leading to the exclusion of those events for determining the size or concentration of the samples (Figure 3g). Using cryo-TEM we show the lipid-bilayer structure of the P10 and P100 fractions, in BEC and LEC-derived EVs (Figure 3h).

3.4 | MiRNA detection in extracellular vesicles

The characterised small EVs (P100) enriched from the same volume of conditioned medium for all donors were used to extract total RNA and subsequently perform small RNA sequencing. Sequencing depth ranged between 8.6 Mio and 31 Mio reads per sample (Figure S3a). At least 80% of total reads mapped to the human genome (Figure S3b). For HUVEC and LEC-tert 0.5 Mio and 1.2 Mio reads mapped to miRNAs, respectively while for LEC, BEC and HDMEC only between 27,000 to 200,000 reads were found to map against the miRBase reference (Figure S3b). The number of identified distinct mature miRNAs ranged from 357 to 727. One hundred twenty-three miRNAs showed a read count above 10 in all EV samples (Figure S3c). Unsupervised hierarchical clustering of vesicular miRNA expression using pre-filtered vesicular miRNAs resembled the results obtained from intracellular miRNA expression, indicating a high correlation of intra- and extracellular miRNA profiles (Figure 4a). Five miRNAs were significantly differentially expressed in EVs derived from LEC versus BEC with an FDR < 0.05 (Figure 4b). Three of these miRNAs (miR-99a-5p, miR-378-3p and miR-874-3p) showed an, on average, 2-fold higher read count in LEC-derived EVs compared to BEC (Figure 4b,c). With a logCPM expression of around 3 and 3.5 miR-150-5p and miR-216a-3p were found to be secreted in higher levels in BEC. In vivo localization of one LEC and one BEC EV-associated miRNA (miR-378-3p and miR-150-5p, respectively) were successfully detected in blood and lymphatic vasculature in human dermal skin using in situ hybridization (Figure S5). Target prediction was performed to identify potential target genes of the vesicular miRNA cargo. Forty-four mRNAs were found to be targeted non-specifically by miRNAs upregulated in both EC types, indicating a potential subset of non-lineage specific EC miRNA interactions. The prediction analysis resulted in 5 and 28 double-interacted genes for BEC and LEC, respectively (Figure 4d). All potential target genes were used in a GO enrichment analysis to retrieve processes that are impacted by the EC lineage-specific EV miRNA cargo. Highest enrichment scores for BEC related targets were observed to be related to the activation of enzymes and biological processes mainly connected to inflammatory response (Figure 4e). The top significantly enriched BPs

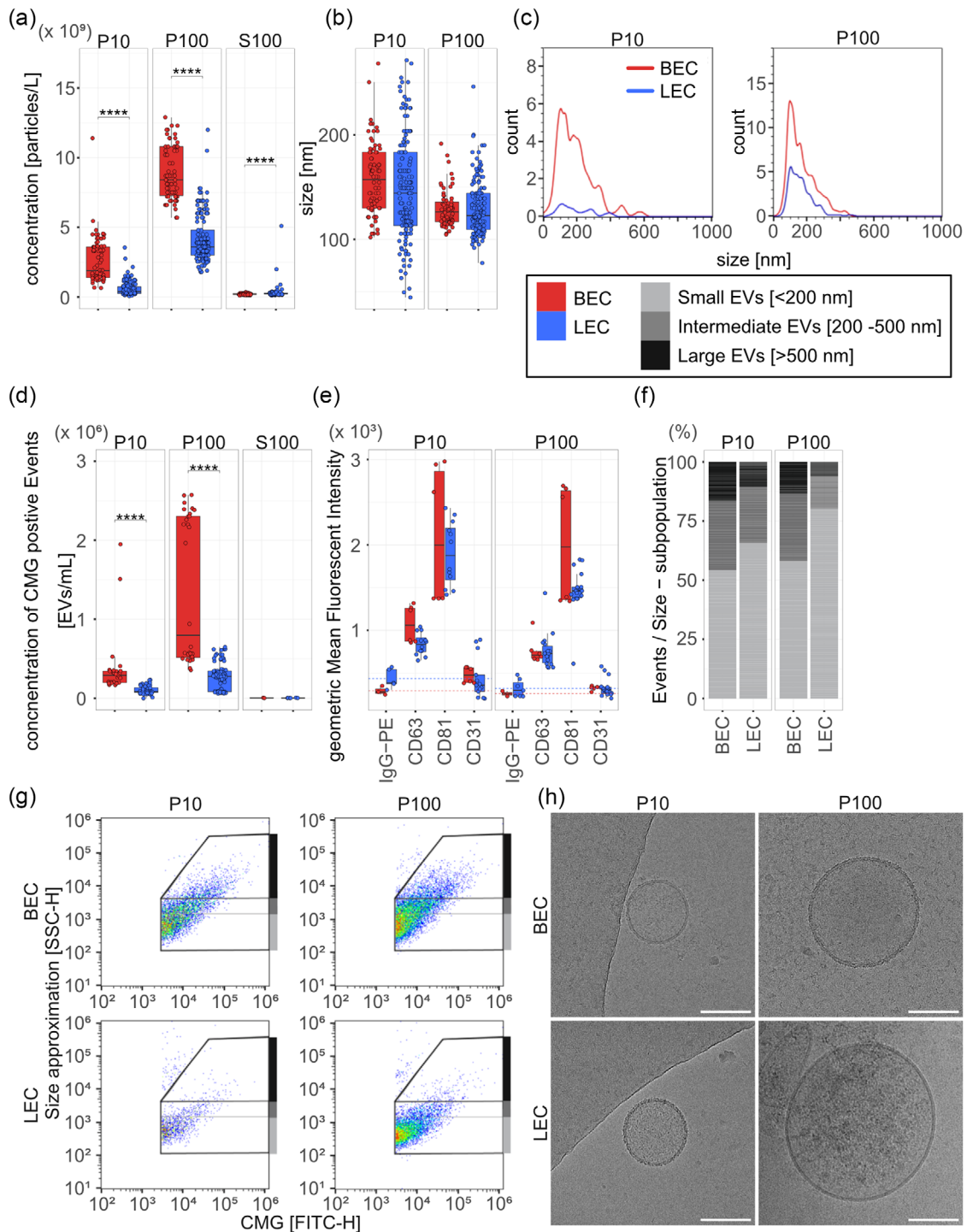


FIGURE 3 Characterization of enriched extracellular vesicles. (a) Concentration and (b) size of the P10 (microvesicle fraction), P100 (small EV fraction) and S100 (supernatant) fraction after the differential ultracentrifugation enrichment protocol. Particles per mL or nm derived from NTA measurements (11 positions, three technical replicates) are plotted for LEC (blue, $n = 5$) and BEC (red, $n = 2$). (c) Representative size distribution histograms for the P10 and P100 fraction from one LEC and BEC donor. (d) Concentration of lipid membrane dye (CMG) stained EVs determined by FITC-triggered flowcytometry. EVs/mL are plotted for 14 technical replicates for LEC (blue, $n = 5$) and BEC (red, $n = 2$). (e) Box plots of the mean fluorescence intensity (MFI) of EV markers (tetraspanins CD81, CD63), endothelial cell surface marker (CD31) and the isotype control detected for CMG-positive events for the P10 and P100 fraction. Dashed lines are the average MFI of the isotype controls for LEC ($n = 5$) and BEC ($n = 2$). (f) Percentage of events detected in the respective size range gate of small EVs (grey, <200 nm), intermediate EVs (middle grey, 200–500 nm) and large EVs (dark grey, >500 nm). Data is derived from 14 technical replicates of CMG-stained P10 and P100 fraction derived from LEC ($n = 5$) and BEC ($n = 2$). (g) Representative scatter plots for P10 and P100 fraction derived from one LEC and BEC donor. (h) Representative cryo-TEM images of EV enriched fractions P10 and P100 from LEC and BEC (Scale Bar = 100 nm).

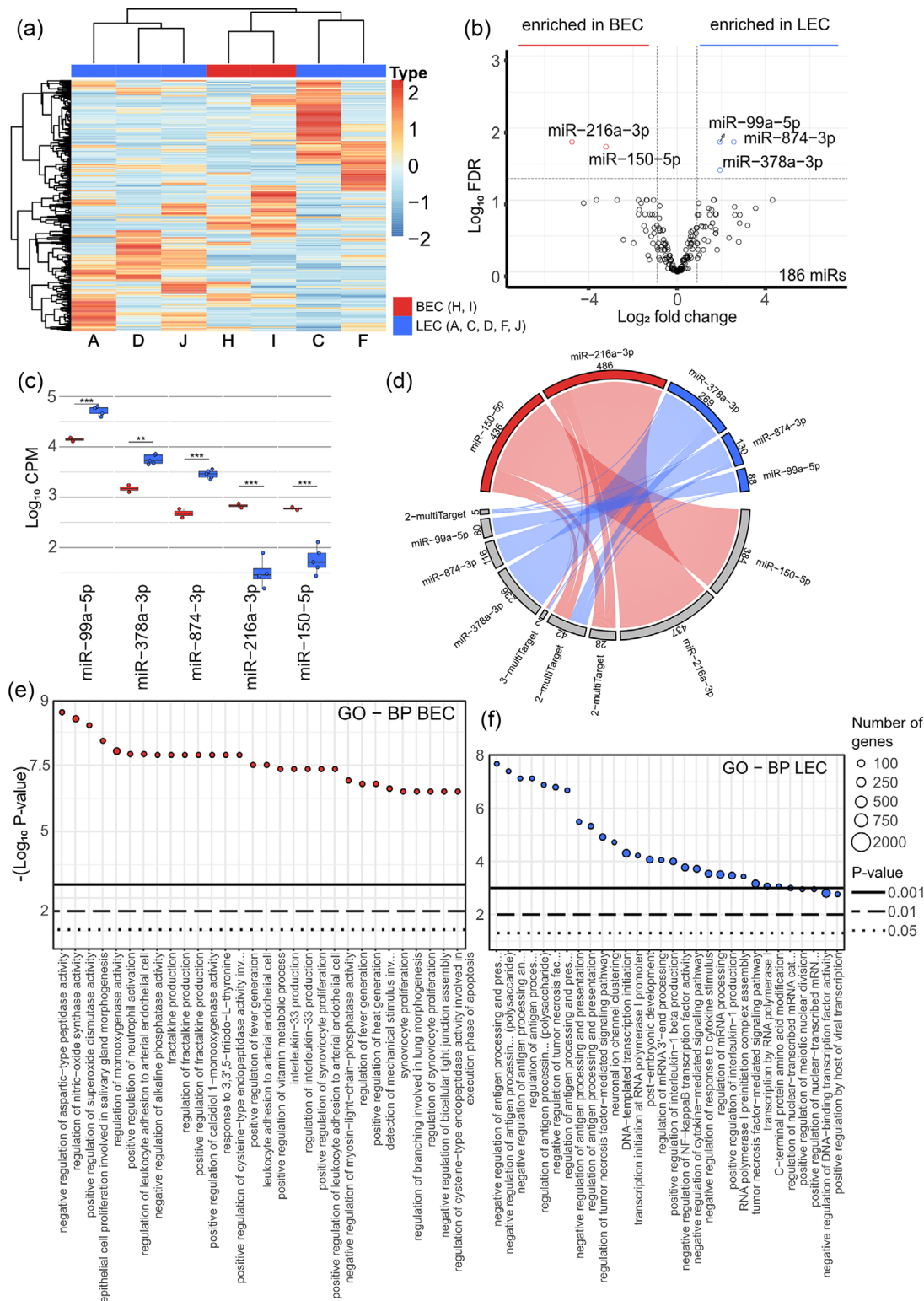


FIGURE 4 Micro RNA associated with extracellular vesicles. (a) Unsupervised hierarchical clustering of miRNA expression for LEC (n = 5) and BEC (n = 2) donors. Clustering is based on unit variance scaled RPM values. Cell type is colour coded on the horizontal clusters. (b) Volcano plot of differential expression of miRNAs between EVs derived from LEC (n = 5) and BEC (n = 2) donors. Log₂ fold change (logFC) and log₁₀ false discovery rate (logFDR) are plotted for 186 miRNAs. Coloured miRNAs were found with a logFC < -1 or > 1 between BEC and LEC (red and blue, respectively). Dashed lines are indicating a FDR > 0.05 and a logFC < -1 or > 1. (c) Box plots of the expression of miRNA found to be differentially expressed. Counts per million are visualized on a log scale for LEC and BEC (blue and red, respectively). Statistics are derived from edgeR (ns p > 0.05, * p < 0.05, ** p < 0.01, *** p < 0.001, **** p < 0.0001). (d) Circos plot visualizing the interaction between upregulated miRNAs in BEC (red) or LEC (blue) and the predicted target mRNAs (grey). Target mRNAs are summarized by the number of interacting miRNAs (e.g., 3-multiTarget contains genes that are targeted by three different miRNAs) and the number

(Continues)

FIGURE 4 (Continued)

of genes per group is provided next to the track. GO-Term enrichment analysis of biological processes for predicted targets of enriched miRNA in (e) BEC and (f) LEC. Top 30 GO-terms found to be enriched for the differentially expressed miRNAs and their predicted targets and their enrichment score (log *p*-value based on Fisher hypergeometric test) is shown. The size of the circle indicated the number of annotated genes per GO-Term. Biological processes related to vascular biology are highlighted in orange.

for LEC secreted miRNA targets are connected to the regulation of MHC-Class II. Further other immune response associated GO-terms were found under the top significantly enriched biological processes (Figure 4f).

3.5 | Correlation of intracellular and vesicular miRNA levels to identify secretion of distinct miRNAs

In order to compare the results of the small RNA sequencing not only on a relative or RPM based level, the spike-in normalized absolute concentrations is used. The comparison and correlation of miRNA expression levels of cells and their corresponding released EVs was used to identify highly abundant and possibly specifically loading of distinct miRNAs. The analysis revealed differences in the miRNAs which are present either intracellularly or extracellularly in association with the EV enriched samples (Figure 5a,b). A subset of highly abundant miRNAs in EVs was identified with an absolute logFC greater than 2. The correlation of miRNAs found in both LEC and BEC EVs showed cell type specific loading patterns of the beforementioned vesicular miRNA species (Figure 5c,d). A selection of three miRNAs which may specifically be loaded into EVs (miR-4488, miR-3960 and miR-4516) was validated via qPCR. RNA, cDNA and qPCR spike-ins confirmed consistent sample processing (Figure S4b). Relative to miR-140-3p normalized Cq values between EVs and cells showed significantly higher expression of the selected miRNAs in EVs for EC samples. Additionally, two out of the three miRNAs (miR-4516 and miR-3960) were detected to be significantly higher abundant in EVs of other cell types (ASC, HFF). Whereas miR-4488 showed a tendency to be associated to EVs but was not significant (Figure S4a). Detailed sequencing mapping statistics for cellular and vesicular samples are shown in Figure S3. In total, 2646 predicted target genes were identified for the potential actively loaded miRNA cargo (Figure 5e). Those target genes were used in a GO enrichment analysis to gain information on their potential impact on BPs. Under the top 30 significantly enriched GO-terms we found several processes associated with the cellular defense response as well as the immune system and senescence (Figure 5f).

4 | DISCUSSION

Our data provide evidence for the secretory behaviour of two different in vitro cultured endothelial cell types. To obtain results which reflect human biology as close as possible, primary human dermal microvascular blood and lymphatic endothelial cells (HDMEC) were chosen. To get a comprehensive picture of the intracellular molecular landscape we measured and analysed cell specific mRNA and miRNA expression profiles. Further insight into potentially long-distance signalling was obtained by characterizing the miRNA cargo derived from cell specific EVs. To provide reliable verdicts which are lymphatic endothelial cell (LEC) and blood endothelial cell (BEC) specific, cells were characterized for endothelial cell type specific surface marker proteins. PECAM-1 (CD31) was to this end chosen as an endothelial cell specific marker, while the presence of Podoplanin (PDPN) was used to identify the lymph-specific phenotype. Cell phenotype was investigated before and after the conditioning process. The latter assessment verified that the EC phenotype was preserved, despite the stress which is inevitably induced by cell conditioning. After enrichment of EVs by ultracentrifugation we applied nanoparticle tracking analysis (NTA) and fluorescence-triggered flow cytometry (FT-FC) (Oesterreicher et al., 2020) for verification in accordance to the MISEV guidelines (Théry et al., 2018). The success of this approach could be verified by finding that more than 90% of the enriched EVs are in the size range below 200 nm. The presence of intact EVs was confirmed by FT-FC which showed successful incorporation of a fluorescent dye (CMG) into the lipid membrane and identified EV and EC specific surface marker proteins. A first characterization revealed that the EVs which were derived from LEC and BEC differ in size and concentration. These distinct differences may hint towards a specialized regulation of EV release behaviour based on the differences in their physiological role and the resulting difference in their gene expression patterns. With the change of EV loading and release endothelial cells could actively alter and change the rate and effectiveness of their paracrine communication.

LEC and BEC specific mRNA profiles were obtained by mRNA sequencing and confirm previous results by Keuschnigg et al. (Keuschnigg et al., 2013) and Tacconi et al. (Tacconi et al., 2021). Confirmation of cell identity was deemed successful as certain genes, such as PROX-1 and PDPN, which are known to be lymph specific (Hirakawa et al., 2003; Nelson et al., 2007) were found to be upregulated in LEC. As expected, we found VEGFC, which is an essential signal from BEC to LEC to stimulate tip cell

FIGURE 5 (Continued)

(colour gradient purple to blue) and the predicted target mRNAs (grey). Target mRNAs are summarized by the number of interacting miRNAs (e.g., 3-multiTarget contains genes that are targeted by three different miRNAs) and the number of genes per group is provided next to the track. (f) GO enrichment analysis of biological processes for predicted targets of top enriched miRNAs. Top 30 GO-terms found to be enriched are visualized by plotting their enrichment score (log *p*-value based on Fisher hypergeometric test). The size of the circle indicated the number of annotated genes per GO-Term. Biological processes related to vascular biology are highlighted in orange.

formation in lymphatic vessels (Rauniyar et al., 2018), to be upregulated in BEC. With these results we ensured a frame of specific gene expression patterns to enable cell type specificity of our data and the subsequent interpretation of physiological relevance.

Due to the importance of the vasculature in many physiological and pathological processes, the specifically and early identification of diseased lymphatic or blood vascular structures in the human body is of high advantage. The identification and characterization of differences in the secretory behaviour of the physiological state of in vitro cultured cells was used to identify potential signatures which later can be used to differentiate between these two vascular systems. Such tissue specific signatures can hold great potential for the identification of biomarker or EVs and their transcriptome in non to little invasive liquid biopsies such as blood (plasma or serum).

Our results show that communication of LEC and BEC differs in terms of EV secretion and miRNA loading which subsequently influences downstream target cells and pathways. Findings like the predominant secretion of miR-378-3p by LEC and miR-216-3p and miR-150-5p by BEC, suggest that further studies should assess the potential use of these miRNAs as potential candidates for biomarkers of various pathological and physiological processes possibly in the context of the specific vascular bed of origin. For example, miR-378-3p as one of the mature forms of the miR-378a family has already been described to actively influence angiogenesis in both healthy tissue as well as in cancer (Krist et al., 2015) and might therefore be a feasible target for analysis of EV based biopsies from various body liquids. EV-based diagnostics might also be feasible for health screenings in pregnancy as it can be performed using almost all body fluids. A target for such a screening might be miR-150-5p, which we were able to successfully detect in EVs derived from BEC. While miR-150-5p is thought to play a role in the differentiation process of endothelial progenitor cells it has also been shown to be upregulated when endothelial cells were exposed to alcohol and adversely affected development of the cortical microvasculature (Du et al., 2020; Perales et al., 2022). Therefore, the potential usage of this miRNA as a marker for fetal alcohol spectrum disorders might be used to specify the impact of the parental alcohol abuse on the foetus. The quantification of EV dependent release of miR-216a by BEC, as we have seen in our study, could potentially be linked to before reported endothelial dysfunction (Menghini et al., 2014) and may be used for early recognition of disease onset of the cardiovascular disease.

The usage of an absolute normalization approach provided the possibility to identify a subset of potentially actively secreted miRNAs by comparing intracellular and extravesicular miRNA concentration. Our current experimental setup indicates that those miRNAs seem to be higher abundant in EVs compared to the overall intracellular presence in EC. The qPCR validation of three selected miRNAs with a high logFC (smaller than -6) between Cell and EV for ECs and a selection of control cells indicated that the identified subset of miRNAs may be secreted actively by other cell types as well hinting towards EV specific miRNA species. All three miRNAs were reported to be associated to EVs not only from EC but for example in plasma derived EVs or in cancer related studies (Umair et al., 2022; Ye et al., 2022; Zhong et al., 2021). MicroRNA miR-3960 was shown to promote the differentiation process of vascular smooth muscle cells into osteoblasts (Xia et al., 2015). This process is typically observed in the medial and intimal layers of blood vessels and the active secretion of miR-3960 induced by, for example, stress can facilitate the vascular calcification via the RUNX2/miR-3960 induced WNT cascade (Jiang et al., 2021; Qin et al., 2021; Tyson et al., 2020). Further investigation of the structure and nucleotide composition of this EV-specific subset of potentially actively secreted miRNAs could help to improve loading efficacy and applicability of EV—miRNA therapeutics.

Our data gives first insights into the secretory behaviour of EVs and their miRNA cargo by LEC and BEC and further adds to the relevant yet still sparse knowledge on endothelial EVs and their use in diagnostics (Trisko et al., 2022). This knowledge might be used for the search for fitting biomarkers in a cell-specific context in the future which could be based on the isolation of EVs from quasi non-invasive liquid biopsies. Furthermore, the observed differences between the primary human EC derived from skin to cell lines such as LEC-Tert as well as the juvenile HUVEC, which are still found in many studies concerning blood vessel research are indicating the necessity of an adult EC source for in vitro vascular research.

AUTHOR CONTRIBUTIONS

Marianne Pultar: Conceptualization; data curation; formal analysis; investigation; methodology; writing—original draft; writing—review and editing. **Johannes Oesterreicher:** Conceptualization; formal analysis; investigation; methodology; validation; writing—original draft; writing—review and editing. **Jaana Hartmann:** Investigation; methodology; validation. **Moritz Weigl:** Investigation; software; writing—review and editing. **Andreas Diendorfer:** Software; validation; writing—review and editing. **Katharina Schimek:** Resources; writing—review and editing. **Thomas Heuser:** Methodology; visualization; writing—review and editing. **Marlene Brandstetter:** Methodology; visualization; writing—review and editing. **Johannes Grillari:** Conceptualization; supervision; writing—review and editing. **Peter Sykacek:** Formal analysis; software; supervision; writing—

review and editing. **Matthias Hackl:** Investigation; methodology; software; supervision; validation. **Wolfgang Holnthoner:** Conceptualization; project administration; supervision; writing—original draft; writing—review and editing.

ACKNOWLEDGEMENTS

We thank Marion Gröger (Medical University of Vienna, tragically passed away recently) for telomerase-immortalized LEC. The Electron Microscopy Facility of the Vienna Bio Center Core Facilities gratefully acknowledges funding by the Austrian Federal Ministry of Education, Science and Research and the City of Vienna. Bertram Aschenbrenner and Beate Lichtenberger (Medical University of Vienna) are acknowledged for providing human skin samples.

CONFLICT OF INTEREST STATEMENT

Johannes Grillari is cofounder and shareholder of Evercyte GmbH and TAmiRNA GmbH. Matthias Hackl is co-founder, shareholder and employee of TAmiRNA GmbH, Marianne Pultar and Andreas Diendorfer are employed at TAmiRNA. All other authors of this manuscript declare no conflicts of interest.

DATA AVAILABILITY STATEMENT

All raw files from RNA analyses will be available in the gene expression omnibus (GEO) under accession number (GSE232379).

ORCID

Wolfgang Holnthoner  <https://orcid.org/0000-0001-6425-9028>

REFERENCES

- Adrian Alexa, J. R. (2017). topGO. Bioconductor. <https://doi.org/10.18129/B9.BIOC.TOPGO>
- Agarwal, V., Bell, G. W., Nam, J. W., & Bartel, D. P. (2015). Predicting effective microRNA target sites in mammalian mRNAs. *Elife*, 4, e05005. <https://doi.org/10.7554/eLife.05005>
- Bushnell, B. (2014). BMAP A Fast, Accurate, Splice-Aware Aligner, März 2014, [Online]. Verfügbar unter: <https://www.osti.gov/biblio/1241166>
- Carlson, M. (2017). org.Hs.eg.db. Bioconductor. <https://doi.org/10.18129/B9.BIOC.ORG.HS.EG.DB>
- Chen, X., Liang, H., Zhang, J., Zen, K., & Zhang, C. Y. (2012). Horizontal transfer of microRNAs: Molecular mechanisms and clinical applications. *Protein & Cell*, 3(1), 28–37. <https://doi.org/10.1007/s13238-012-2003-z>
- Cueni, L. N., & Detmar, M. (2008). The lymphatic system in health and disease. *Lymphatic Research and Biology*, 6(3-4), 109–122. <https://doi.org/10.1089/lrb.2008.1008>
- Diendorfer, A., Khamina, K., Pultar, M., & Hackl, M. (2022). miND (miRNA NGS Discovery pipeline): a small RNA-seq analysis pipeline and report generator for microRNA biomarker discovery studies. *Fl000Research*, 24. February 2022. <https://doi.org/10.12688/fl000research.94159.1>
- Dittrich, T., Köhrer, S., Schorb, M., Haberbosch, I., Börmel, M., Goldschmidt, H., Pajor, G., Müller-Tidow, C., Raab, M. S., Hegenbart, U., Schönland, S. O., Schwab, Y., & Krämer, A. (2022). A high-throughput electron tomography workflow reveals over-elongated centrioles in relapsed/refractory multiple myeloma. *Cell Reports Methods*, 2(11), 100322. <https://doi.org/10.1016/j.crmeth.2022.100322>
- Dobin, A., Davis, C. A., Schlesinger, F., Drenkow, J., Zaleski, C., Jha, S., Batut, P., Chaisson, M., & Gingeras, T. R. (2013). STAR: Ultrafast universal RNA-seq aligner. *Bioinformatics (Oxford, England)*, 29(1), 15–21. <https://doi.org/10.1093/bioinformatics/bts635>
- Du, X., Hu, N., Yu, H., Hong, L., Ran, F., Huang, D., Zhou, M., Li, C., & Li, X. (2020). miR-150 regulates endothelial progenitor cell differentiation via Akt and promotes thrombus resolution. *Stem Cell Research & Therapy*, 11(1), 354. <https://doi.org/10.1186/s13287-020-01871-9>
- Dunworth, W. P., Cardona-Costa, J., Bozkulak, E. C., Kim, J. D., Meadows, S., Fischer, J. C., Wang, Y., Cleaver, O., Qyang, Y., Ober, E. A., & Jin, S. W. (2014). Bone morphogenetic protein 2 signaling negatively modulates lymphatic development in vertebrate embryos. *Circulation Research*, 114(1), 56–66. <https://doi.org/10.1161/CIRCRESAHA.114.302452>
- Ewels, P., Magnusson, M., Lundin, S., & Käller, M. (2016). MultiQC: Summarize analysis results for multiple tools and samples in a single report. *Bioinformatics (Oxford, England)*, 32(19), 3047–3048. <https://doi.org/10.1093/bioinformatics/btw354>
- Feng, W., Chen, L., Nguyen, P. K., Wu, S. M., & Li, G. (2019). Single cell analysis of endothelial cells identified organ-specific molecular signatures and heart-specific cell populations and molecular features. *Frontiers in Cardiovascular Medicine*, 6, 165. <https://doi.org/10.3389/fcvm.2019.00165>
- Flavahan, N. A. (2017). In development—a new paradigm for understanding vascular disease. *Journal of Cardiovascular Pharmacology*, 69(5), 248–263. <https://doi.org/10.1097/FJC.0000000000000480>
- Friedländer, M. R., Chen, W., Adamidi, C., Maaskola, J., Einspanier, R., Knespel, S., & Rajewsky, N. (2008). Discovering microRNAs from deep sequencing data using miRDeep. *Nature Biotechnology*, 26(4), 407–415. <https://doi.org/10.1038/nbt1394>
- Greenspan, L. J., & Weinstein, B. M. (2021). To be or not to be: Endothelial cell plasticity in development, repair, and disease. *Angiogenesis*, 24(2), 251–269. <https://doi.org/10.1007/s10456-020-09761-7>
- Griffiths-Jones, S., Saini, H. K., van Dongen, S., & Enright, A. J. (2008). miRBase: Tools for microRNA genomics. *Nucleic Acids Research*, 36(Database issue), D154–D158. <https://doi.org/10.1093/nar/gkm952>
- Gu, Z., Gu, L., Eils, R., Schlesner, M., & Brors, B. (2014). Circlize implements and enhances circular visualization in R. *Bioinformatics (Oxford, England)*, 30(19), 2811–2812. <https://doi.org/10.1093/bioinformatics/btu393>
- Gurevich, D. B., David, D. T., Sundaraman, A., & Patel, J. (2021). Endothelial heterogeneity in development and wound healing. *Cells*, 10(9), 2338. <https://doi.org/10.3390/cells10092338>
- Guyen, G., Hilty, M. P., & Ince, C. (2020). Microcirculation: Physiology, pathophysiology, and clinical application. *Blood Purification*, 49(1-2), 143–150. <https://doi.org/10.1159/000503775>
- Hammond, S. M., Bernstein, E., Beach, D., & Hannon, G. J. (2000). An RNA-directed nuclease mediates post-transcriptional gene silencing in *Drosophila* cells. *Nature*, 404(6775), 293–296. <https://doi.org/10.1038/35005107>

- Hirakawa, S., Hong, Y. K., Harvey, N., Schacht, V., Matsuda, K., Libermann, T., & Detmar, M. (2003). Identification of vascular lineage-specific genes by transcriptional profiling of isolated blood vascular and lymphatic endothelial cells. *The American Journal of Pathology*, *162*(2), 575–586. [https://doi.org/10.1016/S0002-9440\(10\)63851-5](https://doi.org/10.1016/S0002-9440(10)63851-5)
- Jambusaria, A., Hong, Z., Zhang, L., Srivastava, S., Jana, A., Toth, P. T., Dai, Y., Malik, A. B., & Rehman, J. (2020). Endothelial heterogeneity across distinct vascular beds during homeostasis and inflammation. *Elife*, *9*, e51413. <https://doi.org/10.7554/eLife.51413>
- Jiang, W., Zhang, Z., Li, Y., Chen, C., Yang, H., Lin, Q., Hu, M., & Qin, X. (2021). The cell origin and role of osteoclastogenesis and osteoblastogenesis in vascular calcification. *Frontiers in Cardiovascular Medicine*, *8*, 639740. <https://doi.org/10.3389/fcvm.2021.639740>
- Jung, H. M., Hu, C. T., Fister, A. M., Davis, A. E., Castranova, D., Pham, V. N., Price, L. M., & Weinstein, B. M. (2019). MicroRNA-mediated control of developmental lymphangiogenesis. *Elife*, *8*, e46007. <https://doi.org/10.7554/eLife.46007>
- Keuschnigg, J., Karinen, S., Auvinen, K., Irjala, H., Mpindi, J. P., Kallioniemi, O., Hautaniemi, S., Jalkanen, S., & Salmi, M. (2013). Plasticity of blood- and lymphatic endothelial cells and marker identification. *PLoS ONE*, *8*(9), e74293. <https://doi.org/10.1371/journal.pone.0074293>
- Khamina, K., Diendorfer, A. B., Skalicky, S., Weigl, M., Pultar, M., Krammer, T. L., Fournier, C. A., Schofield, A. L., Otto, C., Smith, A. T., Buchtele, N., Schoergenhofer, C., Jilma, B., Frank, B. J. H., Hofstaetter, J. G., Grillari, R., Grillari, J., Ruprecht, K., Goldring, C. E., ... Hackl, M. (2022). A microRNA next-generation-sequencing discovery assay (miND) for genome-scale analysis and absolute quantitation of circulating microRNA biomarkers. *International Journal of Molecular Sciences*, *23*(3), 1226. <https://doi.org/10.3390/ijms23031226>
- Kriehuber, E., Breiteneder-Geleff, S., Groeger, M., Soleiman, A., Schoppmann, S. F., Stingl, G., Kerjaschki, D., & Maurer, D. (2001). Isolation and characterization of dermal lymphatic and blood endothelial cells reveal stable and functionally specialized cell lineages. *The Journal of Experimental Medicine*, *194*(6), 797–808. <https://doi.org/10.1084/jem.194.6.797>
- Krist, B., Florczyk, U., Pietraszek-Gremplewicz, K., Józkwicz, A., & Dulak, J. (2015). The role of miR-378a in metabolism, angiogenesis, and muscle biology. *International Journal of Endocrinology*, *2015*, 281756. <https://doi.org/10.1155/2015/281756>
- Lall, S., Grün, D., Krek, A., Chen, K., Wang, Y. L., Dewey, C. N., Sood, P., Colombo, T., Bray, N., Macmenamin, P., Kao, H. L., Gunsalus, K. C., Pachter, L., Piano, F., & Rajewsky, N. (2006). A genome-wide map of conserved microRNA targets in *C. elegans*. *Current Biology: CB*, *16*(5), 460–471. <https://doi.org/10.1016/j.cub.2006.01.050>
- Lee, S., Choi, I., & Hong, Y. K. (2010). Heterogeneity and plasticity of lymphatic endothelial cells. *Seminars in Thrombosis and Hemostasis*, *36*(3), 352–361. <https://doi.org/10.1055/s-0030-1253457>
- Love, M. I., Huber, W., & Anders, S. (2014). Moderated estimation of fold change and dispersion for RNA-seq data with DESeq2. *Genome Biology*, *15*(12), 550. <https://doi.org/10.1186/s13059-014-0550-8>
- Maciej Pajak, T. I. S. (2017). miRNAatop. Bioconductor. <https://doi.org/10.18129/B9.BIOC.MIRNATAP>
- Maragkakis, M., Reczko, M., Simossis, V. A., Alexiou, P., Papadopoulos, G. L., Dalamagas, T., Giannopoulos, G., Goumas, G., Koukis, E., Kourtis, K., Vergoulis, T., Koziris, N., Sellis, T., Tsanakas, P., & Hatzigeorgiou, A. G. (2009). DIANA-microT web server: Elucidating microRNA functions through target prediction. *Nucleic Acids Research*, *37*(Web Server issue), W273–W276. <https://doi.org/10.1093/nar/gkp292>
- Menghini, R., Casagrande, V., Marino, A., Marchetti, V., Cardellini, M., Stoehr, R., Rizza, S., Martelli, E., Greco, S., Mauriello, A., Ippoliti, A., Martelli, F., Lauro, R., & Federici, M. (2014). MiR-216a: A link between endothelial dysfunction and autophagy. *Cell Death & Disease*, *5*(1), e1029. <https://doi.org/10.1038/cddis.2013.556>
- Milasan, A., Tessandier, N., Tan, S., Brisson, A., Boilard, E., & Martel, C. (2016). Extracellular vesicles are present in mouse lymph and their level differs in atherosclerosis. *Journal of Extracellular Vesicles*, *5*, 31427. <https://doi.org/10.3402/jev.v5.31427>
- Nelson, G. M., Padera, T. P., Garkavtsev, I., Shioda, T., & Jain, R. K. (2007). Differential gene expression of primary cultured lymphatic and blood vascular endothelial cells. *Neoplasia (New York, N.Y.)*, *9*(12), 1038–1045. <https://doi.org/10.1593/neo.07643>
- Oesterreicher, J., Pultar, M., Schneider, J., Mühleder, S., Zipperle, J., Grillari, J., & Holthöner, W. (2020). Fluorescence-based nanoparticle tracking analysis and flow cytometry for characterization of endothelial extracellular vesicle release. *International Journal of Molecular Sciences*, *21*(23), 9278. <https://doi.org/10.3390/ijms21239278>
- Oliver, G., Kipnis, J., Randolph, G. J., & Harvey, N. L. (2020). The lymphatic vasculature in the 21st century: Novel functional roles in homeostasis and disease. *Cell*, *182*(2), 270–296. <https://doi.org/10.1016/j.cell.2020.06.039>
- Pan, Y., Abdureyim, M., Yao, Q., & Li, X. (2021). Analysis of differentially expressed genes in endothelial cells following tumor cell adhesion, and the role of PRKAA2 and miR-124-3p. *Frontiers in Cell and Developmental Biology*, *9*, 604038. <https://doi.org/10.3389/fcell.2021.604038>
- Pedrioli, D. M., Karpanen, T., Dabouras, V., Jurisic, G., van de Hoek, G., Shin, J. W., Marino, D., Kälin, R. E., Leidel, S., Cinelli, P., Schulte-Merker, S., Brändli, A. W., & Detmar, M. (2010). miR-31 functions as a negative regulator of lymphatic vascular lineage-specific differentiation in vitro and vascular development in vivo. *Molecular and Cellular Biology*, *30*(14), 3620–3634. <https://doi.org/10.1128/MCB.00185-10>
- Perales, G., Westenskow, M., Gutierrez, R., Caldwell, K. K., Allan, A. M., & Gardiner, A. S. (2022). MicroRNA-150-5p is upregulated in the brain microvasculature during prenatal alcohol exposure and inhibits the angiogenic factor Vezfl. *Alcoholism, Clinical and Experimental Research*, *46*(11), 1953–1966. <https://doi.org/10.1111/acer.14939>
- Priglinger, E., Wurzer, C., Steffenhagen, C., Maier, J., Hofer, V., Peterbauer, A., Nuernberger, S., Redl, H., Wolbank, S., & Sandhofer, M. (2017). The adipose tissue-derived stromal vascular fraction cells from lipedema patients: Are they different? *Cytotherapy*, *19*(7), 849–860. <https://doi.org/10.1016/j.jcyt.2017.03.073>
- Pugsley, M. K., & Tabrizchi, R. (2000). The vascular system. An overview of structure and function. *Journal of Pharmacological and Toxicological Methods*, *44*(2), 333–340. [https://doi.org/10.1016/s1056-8719\(00\)00125-8](https://doi.org/10.1016/s1056-8719(00)00125-8)
- Pultar, M. (2022). *MicroRNA profile of extracellular vesicles derived from lymphatic and blood endothelial cells*. [Master Thesis, University of Natural Resources and Life Sciences].
- Putri, G. H., Anders, S., Pyl, P. T., Pimanda, J. E., & Zanini, F. (2022). Analysing high-throughput sequencing data in Python with HTSeq 2.0. *Bioinformatics (Oxford, England)*, *38*(10), 2943–2945. <https://doi.org/10.1093/bioinformatics/btac166>
- Qin, Z., Liao, R., Xiong, Y., Jiang, L., Li, J., Wang, L., Han, M., Sun, S., Geng, J., Yang, Q., Zhang, Z., Li, Y., Du, H., & Su, B. (2021). A narrative review of exosomes in vascular calcification. *Annals of Translational Medicine*, *9*(7), 579. <https://doi.org/10.21037/atm-20-7355>
- Randolph, G. J., Ivanov, S., Zinselmeyer, B. H., & Scallan, J. P. (2017). The lymphatic system: Integral roles in immunity. *Annual Review of Immunology*, *35*, 31–52. <https://doi.org/10.1146/annurev-immunol-041015-055354>
- Rauniar, K., Jha, S. K., & Jeltsch, M. (2018). Biology of vascular endothelial growth factor C in the morphogenesis of lymphatic vessels. *Frontiers in Bioengineering and Biotechnology*, *6*, 7. <https://doi.org/10.3389/fbioe.2018.00007>
- Robinson, M. D., McCarthy, D. J., & Smyth, G. K. (2010). edgeR: A bioconductor package for differential expression analysis of digital gene expression data. *Bioinformatics (Oxford, England)*, *26*(1), 139–140. <https://doi.org/10.1093/bioinformatics/btp616>

- Schimek, K., Busek, M., Brincker, S., Groth, B., Hoffmann, S., Lauster, R., Lindner, G., Lorenz, A., Menzel, U., Sonntag, F., Walles, H., Marx, U., & Horland, R. (2013). Integrating biological vasculature into a multi-organ-chip microsystem. *Lab on a Chip*, 13(18), 3588–3598. <https://doi.org/10.1039/c3lc50217a>
- Shah, M. Y., & Calin, G. A. (2013). The mix of two worlds: Non-coding RNAs and hormones. *Nucleic Acid Therapeutics*, 23(1), 2–8. <https://doi.org/10.1089/nat.2012.0375>
- Simon, A. (2010). FastQC A quality control tool for high throughput sequence data., 2010, [Online]. Verfügbar unter: <https://www.bioinformatics.babraham.ac.uk/projects/fastqc>
- Tacconi, C., He, Y., Ducoli, L., & Detmar, M. (2021). Epigenetic regulation of the lineage specificity of primary human dermal lymphatic and blood vascular endothelial cells. *Angiogenesis*, 24(1), 67–82. <https://doi.org/10.1007/s10456-020-09743-9>
- The RNACentral Consortium. (2019). RNACentral: A hub of information for non-coding RNA sequences. *Nucleic Acids Research*, 47(D1), D221–D229. <https://doi.org/10.1093/nar/gky1034>
- Théry, C., Witwer, K. W., Aikawa, E., Alcaraz, M. J., Anderson, J. D., Andriantsitohaina, R., Antoniou, A., Arab, T., Archer, F., Atkin-Smith, G. K., Ayre, D. C., Bach, J. M., Bachurski, D., Baharvand, H., Balaj, L., Baldacchino, S., Bauer, N. N., Baxter, A. A., Bebawy, M., ... Zuba-Surma, E. K. (2018). Minimal information for studies of extracellular vesicles 2018 (MISEV2018): A position statement of the International Society for Extracellular Vesicles and update of the MISEV2014 guidelines. *Journal of Extracellular Vesicles*, 7(1), 1535750. <https://doi.org/10.1080/20013078.2018.1535750>
- Treiber, T., Treiber, N., & Meister, G. (2019). Regulation of microRNA biogenesis and its crosstalk with other cellular pathways. *Nature Reviews. Molecular Cell Biology*, 20(1), 5–20. <https://doi.org/10.1038/s41580-018-0059-1>
- Trisko, J., Fleck, J., Kau, S., Oesterreicher, J., & Holnthoner, W. (2022). Lymphatic and blood endothelial extracellular vesicles: A story yet to be written. *Life (Basel, Switzerland)*, 12(5), 654. <https://doi.org/10.3390/life12050654>
- Turchinovich, A., Weiz, L., & Burwinkel, B. (2012). Extracellular miRNAs: The mystery of their origin and function. *Trends in Biochemical Sciences*, 37(11), 460–465. <https://doi.org/10.1016/j.tibs.2012.08.003>
- Tyson, J., Bundy, K., Roach, C., Douglas, H., Ventura, V., Segars, M. F., Schwartz, O., & Simpson, C. L. (2020). Mechanisms of the osteogenic switch of smooth muscle cells in vascular calcification: WNT signaling, BMPs, mechanotransduction, and EndMT. *Bioengineering (Basel, Switzerland)*, 7(3), 88. <https://doi.org/10.3390/bioengineering7030088>
- Umair, Z., Baek, M. O., Song, J., An, S., Chon, S. J., & Yoon, M. S. (2022). MicroRNA-4516 in urinary exosomes as a biomarker of premature ovarian insufficiency. *Cells*, 11(18), 2797. <https://doi.org/10.3390/cells11182797>
- Wolbank, S., Peterbauer, A., Fahrner, M., Hennerbichler, S., van Griensven, M., Stadler, G., Redl, H., & Gabriel, C. (2007). Dose-dependent immunomodulatory effect of human stem cells from amniotic membrane: A comparison with human mesenchymal stem cells from adipose tissue. *Tissue Engineering*, 13(6), 1173–1183. <https://doi.org/10.1089/ten.2006.0313>
- Wong, N., & Wang, X. (2015). miRDB: An online resource for microRNA target prediction and functional annotations. *Nucleic Acids Research*, 43(Database issue), D146–D152. <https://doi.org/10.1093/nar/gku1104>
- Xia, Z. Y., Hu, Y., Xie, P. L., Tang, S. Y., Luo, X. H., Liao, E. Y., Chen, F., & Xie, H. (2015). Runx2/miR-3960/miR-2861 positive feedback loop is responsible for osteogenic transdifferentiation of vascular smooth muscle cells. *BioMed Research International*, 2015, 624037. <https://doi.org/10.1155/2015/624037>
- Ye, P., Mi, Z., Wei, D., Gao, P., Ma, M., & Yang, H. (2022). miR-3960 from mesenchymal stem cell-derived extracellular vesicles inactivates SDC1/Wnt/ β -catenin axis to relieve chondrocyte injury in osteoarthritis by targeting PHLDA2. *Stem Cells International*, 2022, 9455152. <https://doi.org/10.1155/2022/9455152>
- Zerbino, D. R., Achuthan, P., Akanni, W., Amode, M. R., Barrell, D., Bhai, J., Billis, K., Cummins, C., Gall, A., Girón, C. G., Gil, L., Gordon, L., Haggerty, L., Haskell, E., Hourlier, T., Izuogu, O. G., Janacek, S. H., Juettemann, T., To, J. K., ... Flicek, P. (2018). Ensembl 2018. *Nucleic Acids Research*, 46(D1), D754–D761. <https://doi.org/10.1093/nar/gkx1098>
- Zhong, D., Wu, C., Xu, D., Bai, J., Wang, Q., & Zeng, X. (2021). Plasma-derived exosomal hsa-miR-4488 and hsa-miR-1228-5p: Novel biomarkers for dermatomyositis-associated interstitial lung disease with anti-melanoma differentiation-associated protein 5 antibody-positive subset. *BioMed Research International*, 2021, 6676107. <https://doi.org/10.1155/2021/6676107>

SUPPORTING INFORMATION

Additional supporting information can be found online in the Supporting Information section at the end of this article.

How to cite this article: Pultar, M., Oesterreicher, J., Hartmann, J., Weigl, M., Diendorfer, A., Schimek, K., Schädl, B., Heuser, T., Brandstetter, M., Grillari, J., Sykacek, P., Hackl, M., & Holnthoner, W. (2024). Analysis of extracellular vesicle microRNA profiles reveals distinct blood and lymphatic endothelial cell origins. *Journal of Extracellular Biology*, 3, e134. <https://doi.org/10.1002/jex2.134>